surfaces

MDPI

Article

Green Synthesized *Catharanthus roseus* Floral-Assisted Manganese Oxide Nanoparticles: Cytotoxicity, Wound Healing Activity and Antibacterial Properties

Rajiv Periakaruppan [1,*], Hariharan Balamurugan [1], Vanathi Palanimuthu [2], Joaval Antony Martin [1], Danusree Babu [1] and Noura Al-Dayan [3]

[1] Department of Biotechnology, PSG College of Arts & Science, Coimbatore 641014, Tamil Nadu, India; hariharanb.biotech@gmail.com (H.B.); joavalantonybt@gmail.com (J.A.M.); danusreebabu07@gmail.com (D.B.)
[2] Department of Biotechnology, Sri Ramakrishna College of Arts & Science, Coimbatore 641006, Tamil Nadu, India; vanathi.palanimuthu@gmail.com
[3] Department of Medical Lab Sciences, Prince Sattam Bin Abdulaziz University, Alkharj 16278, Saudi Arabia; n.aldayan@psau.edu.sa
* Correspondence: rajivsmart15@gmail.com

Abstract

Green synthesis of metal oxide nanoparticles (NPs) offers an eco-friendly, cost-effective alternative to conventional chemical and physical methods, minimizing energy use and hazardous reagents. This study demonstrates the biogenic production of manganese oxide (MnO) NPs using *Catharanthus roseus* flower extract as a reducing and capping agent, Comprehensive characterization via FTIR (Mn–O vibrations at 591–405 cm^{-1} along the capping groups), XRD (confirms the cubic crystalline phase), FESEM (flaky, agglomerated sheets), EDX (Mn 62.37%, O 28.40% and C 9.23%), zeta potential (−0.3 mV), and TGA (33.7% phased mass loss to 985 °C) verified pure and stable MnO NPs. In vitro assays on L929 fibroblasts revealed dose-dependent MTT cytotoxicity (78.77% viability at 20 µg/mL to 39.97% at 100 µg/mL) yet enhanced scratch wound closure (−16.31% area reduction vs. −17.41% control), alongside potent antibacterial activity with highest inhibition zones of 15 mm against *Klebsiella pneumoniae* and *Escherichia coli*, and lowest of 4 mm against *Pseudomonas aeruginosa* at 40–100 µg/mL. These multifaceted properties highlight *C. roseus*-assisted MnO NPs' promise for wound healing and antimicrobial applications, warranting dosage optimization and in vivo studies.

Keywords: green synthesis; MnO nanoparticle; *Catharanthus roseus*; flower; cytotoxicity; wound healing

Check for updates

Academic Editor: Jinde Zhang

Received: 15 May 2026
Revised: 3 June 2026
Accepted: 9 June 2026
Published: 10 June 2026

Copyright: © 2026 by the authors. Licensee MDPI, Basel, Switzerland. This article is an open access article distributed under the terms and conditions of the Creative Commons Attribution (CC BY) license.

1. Introduction

Nanotechnology is a multidisciplinary field that combines chemistry, engineering, physics and materials science to design, characterize and produce nanoscale materials with controlled structure and size. It focuses on materials that have dimensions smaller than 100 nanometres [1]. At this scale, nanostructured materials and nanocomposites have a wide range of applications and exhibit superior performance compared to their macro or bulk counterparts [2]. Applications of nanotechnology span diverse fields—environmental science [3], agriculture [4], medicine [5] and food technology [6].

Nanoparticles (NPs) play a major role in nanotechnology due to their unique physico-chemical properties and versatile applications [7]. NPs are categorized as zero-dimensional

nanomaterials, differing from one- and two-dimensional nanomaterials that have one or two dimensions beyond the nanoscale. The different unique properties of NPs are size, chemical reactivity, mobility, and energy absorption [8]. Various synthetic strategies and techniques are used to produce NPs. The two main approaches are the bottom-up and top-down approaches [9].

The top-down approach reduces bulk materials into nanosized particles. Simple and reliable, but requires high energy and limited precision in control of particle size and shape [10]. The bottom-up approach involves the assembly of atoms or molecules into NPs using chemical or biological methods. Chemical synthesis is scalable, but requires additional purification to remove residual agents. Biological synthesis offers high stability and biocompatibility [11]. Studies indicate that synthesizing NPs through biological methods is cost-effective and environmentally friendly. So far, various biological agents such as bacteria, fungi, yeast, actinomycetes, and plants have been successfully utilized for NPs production [12].

Plant species serve as a source of raw materials, with extracts obtainable from diverse plant parts including flowers, leaves, branches, fruits, and roots, providing rich bio-reducing substances. Plant-mediated synthesis is an effective strategy for nanotechnology, particularly MnO_2 NPs [13]. Green nanotechnology, a branch of green technology, applies the principles of green chemistry and green engineering where the term "green" means the use of plant-based products for the synthesis of NPs [14]. It emphasizes using nanoscale innovations to increase sustainability, reduce costs, and reduce ecological risks from harmful externalities [15]. The cytotoxicity of green NPs is significantly lower than that of chemically synthesized nanoparticles, indicating that green NPs are biocompatible and suitable for widespread use in biomedical applications [16].

Researchers focus on transition metal NPs, especially their oxides. It has various applications across industries due to the presence of multiple oxidation states that enable varied configurations [17]. Metal and metal oxide nanoparticles (MO NPs) exhibit distinct physicochemical properties including surface, optical, thermal, and electrical characteristics when compared to the bulk counterparts [18]. The reducing agent influences the properties of MO NPs [19]. Manganese (Mn) is a transition metal naturally occurring as the stable isotope ^{55}Mn. It can exist in multiple oxidation states, including +2, +3, +4, +6, and +7, with the +2 state (Mn(II)) being the most common and biologically relevant form [17]. Mn oxides (MnO, Mn_2O_3, Mn_3O_4, MnO_2 and Mn_5O_8) exhibit different structural transformations among 3D transition metal oxides, and show great potential in nanotechnology applications like batteries, catalysts, drug delivery, solar photovoltaic materials, molecular cells, and solar cells [20]. Mn NPs possess diverse biomedical applications, photothermal therapy, fluorescence quenching, biosensors, antimicrobial activity, and anti-angiogenic effects [21]. Previous studies confirm that Mn NPs effectively remove thallium from wastewater, demonstrating high affinity for metal cations [22].

Researchers have reported the green synthesis of MnO NPs using floral extracts of *Matricaria chamomilla* L. [23], *Phaseolus lunatus* [24], *Costus woodsonii* [25] and *Rosa* sp. [26] for antibacterial activity, biofilm inhibition, antimicrobial activity, dye adsorption, and wound healing. The green synthesis of MnO NPs had gained significant attention for utilizing environmentally safe, non-toxic reagents, unlike conventional chemical methods that incorporate hazardous chemicals [27]. Key advantages of MnO NPs include enhanced biocompatibility, precise morphological control, cost-effectiveness, and the natural reducing capabilities of enzymes and proteins from plant extracts [28].

C. roseus belongs to the family Apocynaceae also known as Madagascar periwinkle. It is a perennial herb native to Madagascar and widely cultivated as an ornamental plant. *C. roseus* is 30–60 cm in length with oblong leaves and white to red flowers, and produces

paired follicles as fruit [29]. It is rich in bioactive phytoconstituents such as alkaloids, saponins, carbohydrates, and flavonoids distributed across its roots, bark, leaves, and flowers [30]. *C. roseus* plant notably contains essential indole alkaloids such as vinblastine, vincristine, leurosine, ajmalicine, raubasine, reserpine, vindoline, rosicline, leurosidine, vinconine, vinblastinine, leurocristine, vindolicine, pleurosine, catharanthamine, deoxyvinblastine, vincardine, tabersonine, and roseadine [31]. *C. roseus* exhibits diverse pharmacological properties such as anticancer, antidiabetic, antivirus, and antibacterial effects. Alkaloids like vindoline, vincristine, vinblastine, and catharanthine inhibit cell proliferation by changing its microtubular dynamics causing apoptosis [32].

Despite extensive research on green synthesis of MnO NPs using various plant extracts, MnO NPs remain underexplored, especially in *C. roseus* flower-assisted synthesis, which are primarily used for silver [33], zinc oxide, and copper oxide NPs. While *C. roseus* leaves and whole extracts have demonstrated efficiency in green synthesis of other metal oxides, flower-specific phytochemicals abundant in alkaloids, flavonoids, terpenoids, and phenolics provide a new, environmentally friendly pathway for the synthesis of the MnO NPs. The investigation addresses *C. roseus* flower-assisted MnO NP biosynthesis, comprehensive physicochemical characterization and bioactivity evaluation to exploit their sustainable potential for antibacterial and biomedical applications.

2. Materials and Methods

2.1. Materials

C. roseus flowers were procured from Garden, PSG College of Arts & Science, Coimbatore, Tamil Nadu, India. $MnSO_4 \cdot H_2O$ mol. wt. 169.02 g/mol, NaOH mol. wt. 39.997 g/mol, $\geq$98% purity was purchased from Sigma Aldrich, Mumbai, India.

2.2. Extraction of C. roseus Flower

Fresh flowers of *C. roseus* were rinsed with tap water and distilled water to remove impurities and air-dried at room temperature. The flowers were finely ground into paste using mortar and pestle. Total of 5 g of *C. roseus* flowers were weighed and mixed with 100 mL of double-distilled water. The *C. roseus* mixture was heated in a water bath (90 °C, 25 min). Then it was filtered using Whatman No. 1 filter paper and stored at 4 °C till further use.

2.3. Synthesis of C. roseus Flower-Assisted MnO NPs

A total of 100 mL of *C. roseus* flower extract was added dropwise to 100 mL of 0.1 M $MnSO_4 \cdot H_2O$ under constant magnetic stirring at 80 °C, resulting in a dark brown colour change. Subsequently, 1 M NaOH was added dropwise to adjust the pH to 10 and stirring was continued for 1 h. The mixture was left overnight for complete precipitation and then centrifuged at 1230$\times$ *g* for 10 min using Remi R-8 c plus (12 $\times$ 15 mL), which was used for centrifugation. The collected precipitate was washed repeatedly with distilled water and ethanol by centrifuge, then dried in an oven at 100 °C for 30 min, which promotes the crystallization of MnO NPs (Figure 1).

2.4. Physicochemical Characterization of MnO NPs

2.4.1. UV–Visible Spectroscopy

UV–visible absorption spectroscopy was performed to characterize the optical properties of *C. roseus* flower-assisted MnO NPs. A Shimadzu UV-Biospec nano-spectrophotometer (Shimadzu Corporation, Kyoto, Japan) recorded spectra in the 200–800 nm range using a 1 cm quartz cuvette with deionized water as the blank.

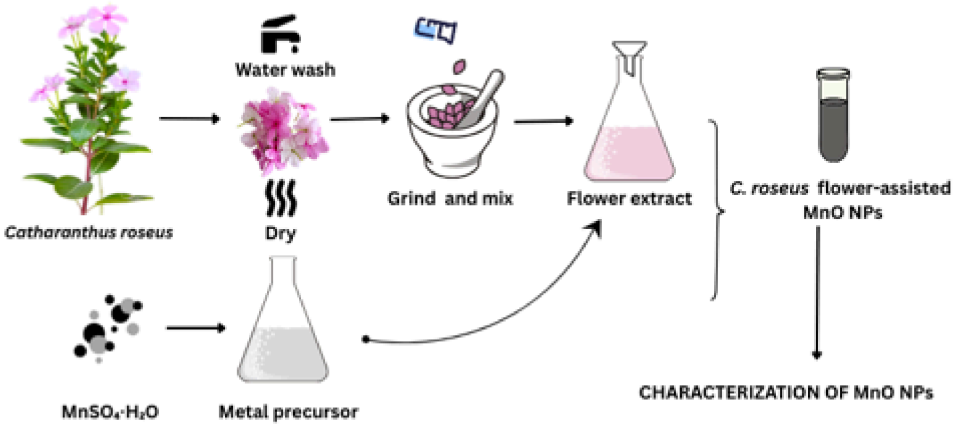


Figure 1. Graphical abstract of *C. roseus* flower-assisted MnO NPs.

2.4.2. FTIR Analysis

FTIR spectroscopy was conducted using a Shimadzu MIRacle 10 spectrophotometer (Shimadzu Corporation, Kyoto, Japan) over 4000–400 cm^{-1}. A small amount of MnO NPs was intimately mixed with anhydrous KBr powder, ground, and pressed into a pellet under vacuum after background acquisition for functional group identification at room temperature.

2.4.3. XRD Analysis

XRD analysis employed an X'Pert Pro PANalytical diffractometer (Malvern Instruments, Almelo, The Netherlands) with Cu Kα radiation (λ = 1.5406 Å, 40 kV, 30 mA) to determine the crystalline nature of the synthesized MnO NPs. Patterns were recorded at 2θ = 30–80° with a step size of 0.02°; phases matched JCPDS data, with crystallite size calculated by the Debye–Scherrer equation:

$$D = \frac{k\lambda}{\beta \cos\theta},$$

The Scherrer constant (k) was taken as 0.9, the wavelength of the X-ray beam (λ) was 0.1541 nm, β represented the full width at half maximum (FWHM) in radians, and θ denoted the Bragg angle.

2.4.4. FESEM-EDX Analysis

Field emission scanning electron microscopy (FESEM) examined particle shape, size, and distribution using a TESCAN MIRA3 XMU (Tescan, Brno, Czech Republic) at magnifications of 10,000–100,000×. EDX spectroscopy, integrated with FESEM, determined the composition and elemental purity.

2.4.5. Zeta Potential and Thermogravimetric Analysis

Zeta potential evaluated stability via electrophoretic mobility in deionized water. TGA was analyzed by thermal decomposition with EXSTAR 6300 (Hitachi High-tech, Oxfordshire, UK) (10 mg sample, 30–985 °C at 10 °C/min under N_2).

2.4.6. Biological Properties

Antibacterial Activity

The antibacterial activity of *C. roseus* flower-assisted MnO NPs was evaluated against Gram-positive (*B. subtilis*) and Gram-negative (*P. aeruginosa*, *E. coli* and *K. pneumoniae*) pathogens using well diffusion method. The bacterial strains were collected from the Department of Microbiology, PSG College of Arts & Science, Coimbatore. Mueller-Hinton

agar was prepared, autoclaved and poured into a sterile Petri plate. Standardized bacterial suspensions were spread evenly across agar surfaces using sterile swabs, the wells were made with a sterile well puncher, and treated with different concentrations of MnO NPs (40, 60, 80, 100 µg/mL) and ofloxacin 5 µg/disc as standard antibiotic. MnO NPs treated plates were incubated at 37 °C for 24 h, after which zones of inhibition were measured in mm.

Cytotoxicity Assay

Cytotoxicity assay of *C. roseus* flower-assisted MnO NPs was conducted against L929 fibroblast cell line. L929 cells were cultured in Dulbecco's Modified Eagle's Medium (DMEM) supplemented with 10% fetal bovine serum (FBS) and penicillin–streptomycin (10 mg/mL) at 37 °C in a 5% CO_2 atmosphere. Cells seeded at 5×10^4 cells/well in 96-well plates with passage number less than 10 were incubated for 24 h to reach 80% confluency. The cells were then treated with varying concentrations (20, 40, 60 and 80 µg/mL) of MnO NPs for 24 h. After treatment, MTT solution (5 mg/mL) was added (20 µL/well) and incubated for 4 h. Formazan crystals were dissolved in DMSO (100 µL/well) and absorbance measured at 570 nm using a microplate reader (Multiskan FC, Thermo Fisher Scientific Inc., Waltham, MA 02451, USA). Untreated cells served as a control. Cell viability was calculated in percentage relative to control and IC_{50} values were determined by probit analysis. All experiments were performed in triplicate.

Scratch (Migration) Assay

The wound healing property of *C. roseus* flower-assisted MnO NPs was examined in vitro using the scratch assay. Confluent monolayers of L929 fibroblasts were grown in 6-well plates with complete DMEM until 90–100% confluence. Uniform linear scratches were created vertically using a sterile 200 µL pipette tip, maintaining a consistent width between wells. Debris was rinsed with PBS and cells treated with 20 µg of MnO NPs in DMEM, using untreated scratches as controls. The plates were incubated for 24 h at 37 °C in 5% CO_2. Wound closure was visualized microscopically at 0 h and 24 h.

2.4.7. Statistical Analysis

All experiments were performed in three independent biological replicates (n = 3 per group) and data were expressed as mean ± standard deviation (SD). Statistical analysis was performed using GraphPad Prism version 10.6.1 (GraphPad Software, San Diego, CA, USA) with two-way ANOVA followed by Dunn's post hoc test for multiple comparisons. Two-way ANOVA evaluated the effects of NP concentration and bacterial strain/time point interactions on zone of inhibition, cell viability, or wound closure. Statistical significance indicated as ** $p < 0.01$, *** $p < 0.001$, **** $p < 0.0001$.

2.4.8. Results and Discussions

UV–Visible Spectroscopy Analysis

The UV–Vis spectrum of the *C. roseus* flower extract showed a strong absorption peak at 230 nm, characteristic of $\pi \rightarrow \pi^*$ and $n \rightarrow \pi^*$ transitions of phenolic and other aromatic phytochemicals. The *C. roseus*-mediated MnO NPs showed a broader, less intense absorption profile extending from 250 to 500 nm, indicating consumption and surface binding of the extract chromophores and confirming successful formation of MnO NPs (Figure 2).

Akpeji et al. [34] reported that MnO_2 NPs synthesized using *Raphia hookeri* seed extract showed maximum UV–Vis absorbance at 421 nm, which confirmed the reduction of manganese acetate precursor to black-coloured MnO_2 NPs. UV–Vis spectroscopy revealed that *Martynia annua* extract reduced 1 mM $KMnO_4$ from magenta-pink to brown overnight in darkness at room temperature, visually indicating MnO_2 NPs formation, with a strong

absorption maximum at 370 nm consistent with prior green synthesis precedents [35]. Alshahrani et al. [36] determined MnV_2O_5 NPs from jasmine flower extract sol–gel synthesis with bandgap Eg = 2.49 eV via Tauc plot extrapolation of $(\alpha h\nu)^2$ vs. $h\nu$.

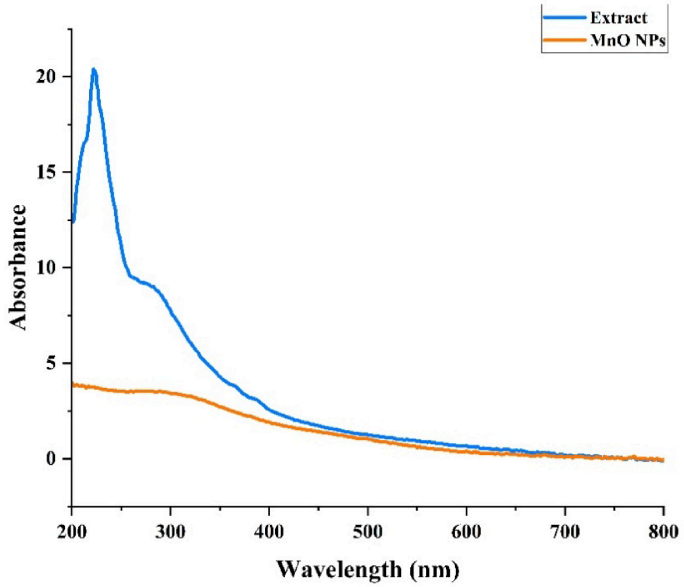


Figure 2. UV–Visible spectrum of *C. roseus* flower-assisted MnO NPs.

FTIR Analysis

C. roseus flower extract exhibited prominent FTIR transmittance peaks (Figure 3a) at 3314 cm^{-1} (O–H/N–H stretching of phenols, alcohols and amines), a cluster of weak bands between 2186 and 1979 cm^{-1} (C≡C/C≡N stretching), and 1635 cm^{-1} (C=O stretching of amide groups and aromatic C=C). Strong bands at 525, 511, 483, 471, 455, 446, 438, 428, 416, 410 and 406 cm^{-1} correspond to C–Br/C–I stretching in alkyl halides and Mn–O vibrations, confirming the presence of bioactive functional groups responsible for MnO NP bioreduction and stabilization. *Caralluma bicolor* aqueous extract phytocompounds revealed eleven FTIR bands at 3452.58 (O-H phenols/alcohols), 3302.13 (N-H primary amines), 2931.80 (C-H alkanes), 2376.30/2229.71 (CO_2/nitriles), 1585.49 (aromatics), 1419.61 (C=C), 1076.28 (C-O alcohols), 655.80/617.22/428.20 cm^{-1} (alkyl halides/alkynes) across 500–4000 cm^{-1} [37].

C. roseus flower-assisted MnO NPs showed FTIR bands at 2922 cm^{-1} (aliphatic C–H stretching), 2159–2112 cm^{-1} (C≡C/C≡N groups), 1978–1861 cm^{-1} (aromatic overtones), 1573 and 1399 cm^{-1} (aromatic C=C and C–N/C–O vibrations), and 1066, 945 and 809 cm^{-1} (C–O/C–N of polysaccharides and proteins). Strong absorptions at 591, 462, 424, 417 and 405 cm^{-1} were assigned to Mn–O lattice vibrations, confirming MnO NP formation with residual *C. roseus* phytochemicals capping the NP surface (Figure 3b). Ogunyemi et al. [23] reported that FTIR spectra of MnO_2 NPs biosynthesized using *Matricaria chamomilla* L. flower extract exhibited characteristic bands at 3386, 1643, 1395, 1056, and 570 cm^{-1}. The broad peak at 3386 cm^{-1} was ascribed to O–H and N–H stretching, 1643 cm^{-1} to C=C/C=O stretching, 1395 cm^{-1} to C–H bending, 1056 cm^{-1} to C–O stretching, and 570 cm^{-1} confirmed the characteristic Mn–O vibration of MnO_2 NPs. Valle-Rivera et al. [38] studied that FTIR spectra of Mn_3O_4 NPs synthesized from *N. oleander* and *B. orellana* leaf extracts revealed characteristic Mn–O vibrations at 477–493 cm^{-1} (octahedral) and 594–608 cm^{-1} (tetrahedral), alongside peaks at 1049–1068 cm^{-1} (Mn–O–H), 1368–1414 cm^{-1} (adsorbed H_2O/CO_2), 1566–1626 cm^{-1} (O–H stretching), and 3207–3330 cm^{-1} (broad hydroxyls).

Higher extract concentrations diminished Mn_3O_4 band clarity, particularly with *B. orellana*, due to increased organic surface coatings.

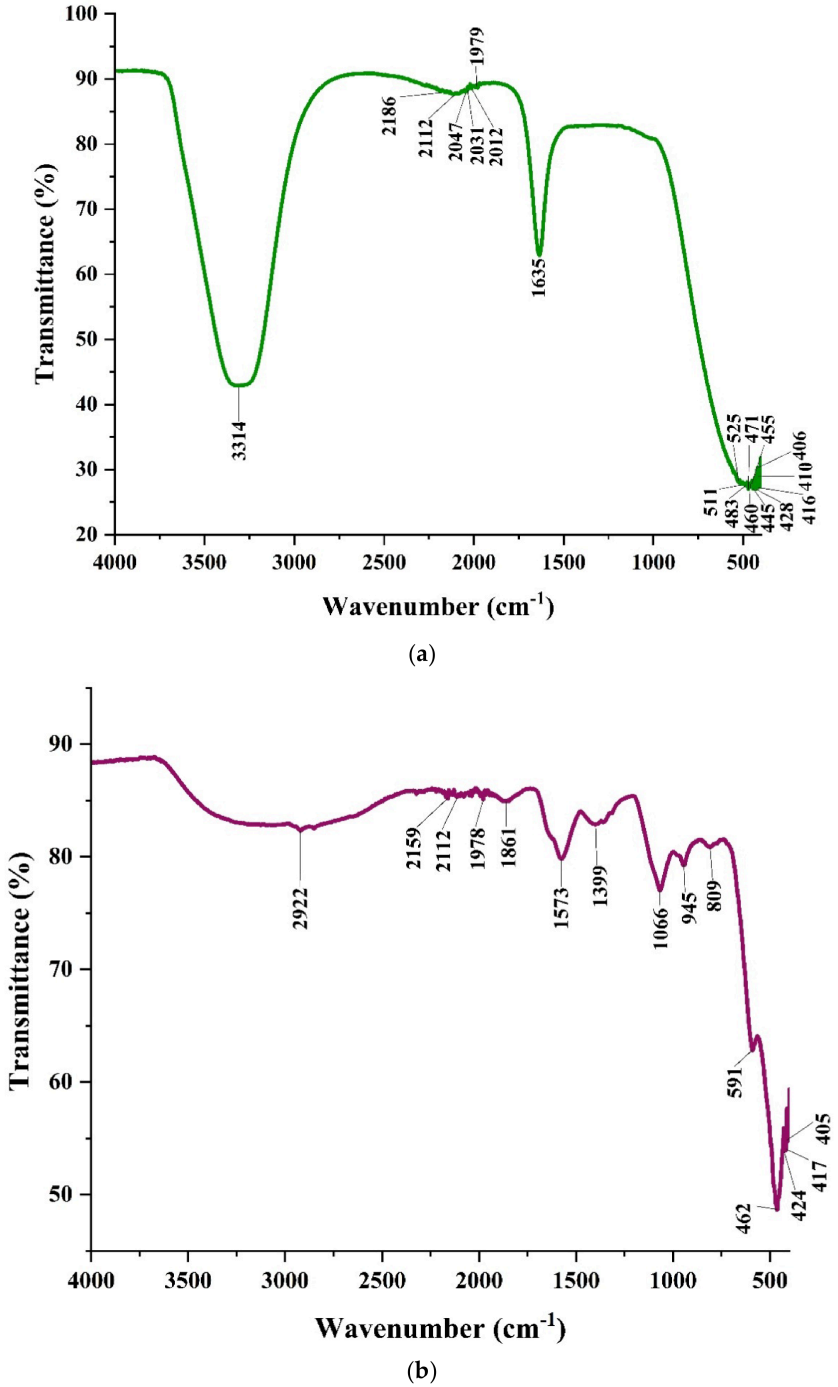


Figure 3. FTIR spectra of (**a**) *C. roseus* flower extract and (**b**) *C. roseus* flower extract-assisted MnO NPs.

XRD Analysis

C. roseus flower-assisted MnO NPs exhibited a broad XRD pattern (Figure 4) in the 2θ range 30–80°, with distinct reflections indexed to the (111), (200), (202), (311) and (222) planes of cubic MnO. The diffractogram matched the standard JCPDS card no. 96-900-6663 for manganosite (MnO). The average crystallite size was calculated as 34 nm using the Debye–Scherrer equation. No extra peaks attributable to impurity phases were detected, confirming the formation of single-phase crystalline MnO NPs.

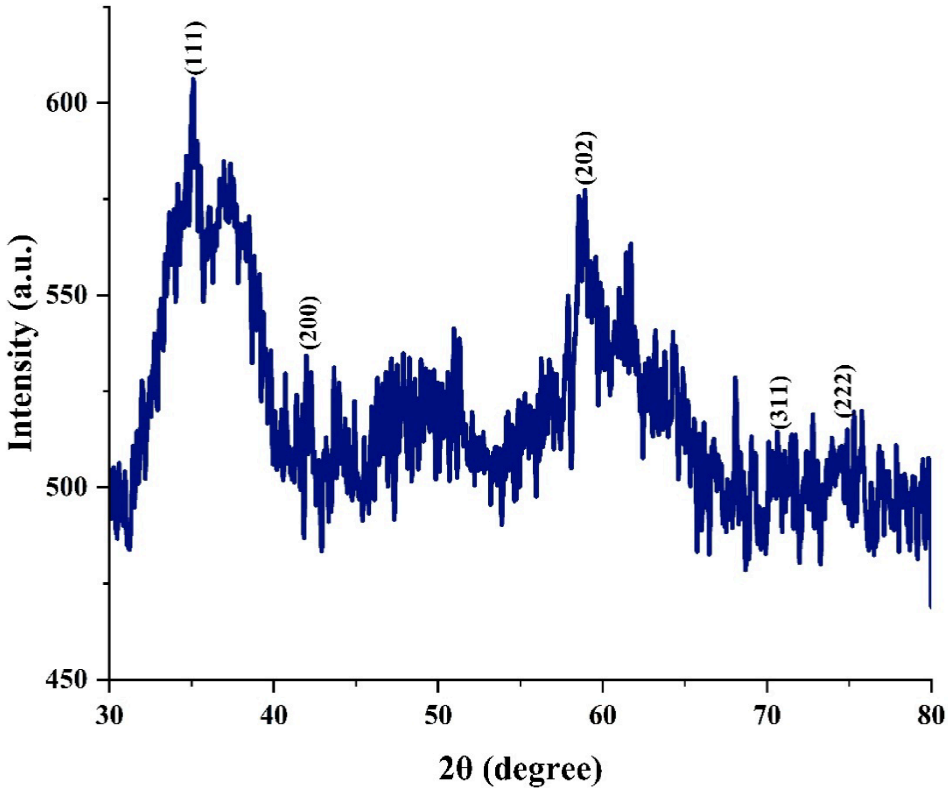


Figure 4. XRD analysis of *C. roseus* flower-assisted MnO NPs.

Dixit et al. [39] performed the XRD analysis of MnO NPs synthesized using *Tinospora cordifolia* stem extract. The diffraction pattern showed prominent peaks at 2θ values of 23.25°, 33.45°, 38.80° and 56.74°, indexed to the (110), (101), (111) and (211) planes consistent with the crystalline structure of MnO NPs. Using the Debye–Scherrer equation, the average crystallite size of MnO NPs was calculated to be 62.59 nm. *Brassica oleracea* leaf-derived MnO NPs were polycrystalline in nature with average crystallite size of 10.70 nm by Debye–Scherrer [40].

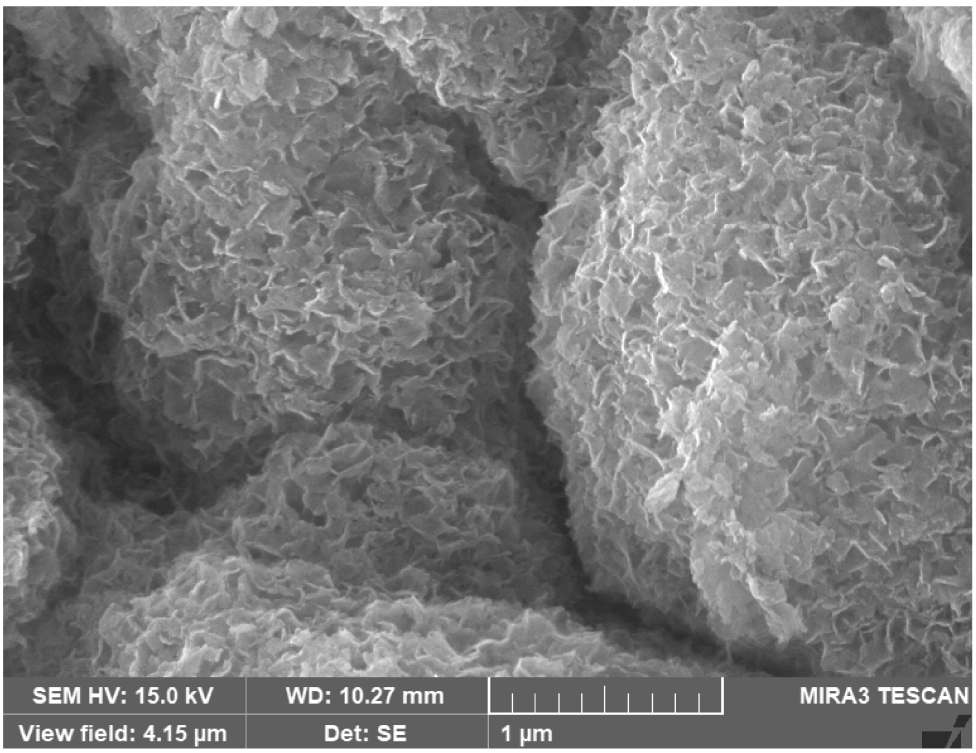
FESEM Analysis

FESEM images revealed that *C. roseus* flower-assisted MnO NPs consisted of densely packed, flaky, crumpled sheet with agglomerated clusters, indicating assemblies of fine nanostructured domains, consistent with high surface area MnO suitable for biological interactions (Figure 5a,b). Kamran et al. [41] displayed that MnO NPs from *Cinnamomum verum* bark extract displayed spherical morphology under SEM, <100 nm in size, and aggregated. SEM images revealed porous, spherical (Mn_3O_4) L (leaf) and (Mn_3O_4) P (petal) NPs from *Tagetes erecta* extract with agglomeration tendency, measuring 14–35 nm diameters consistent with XRD data [42].

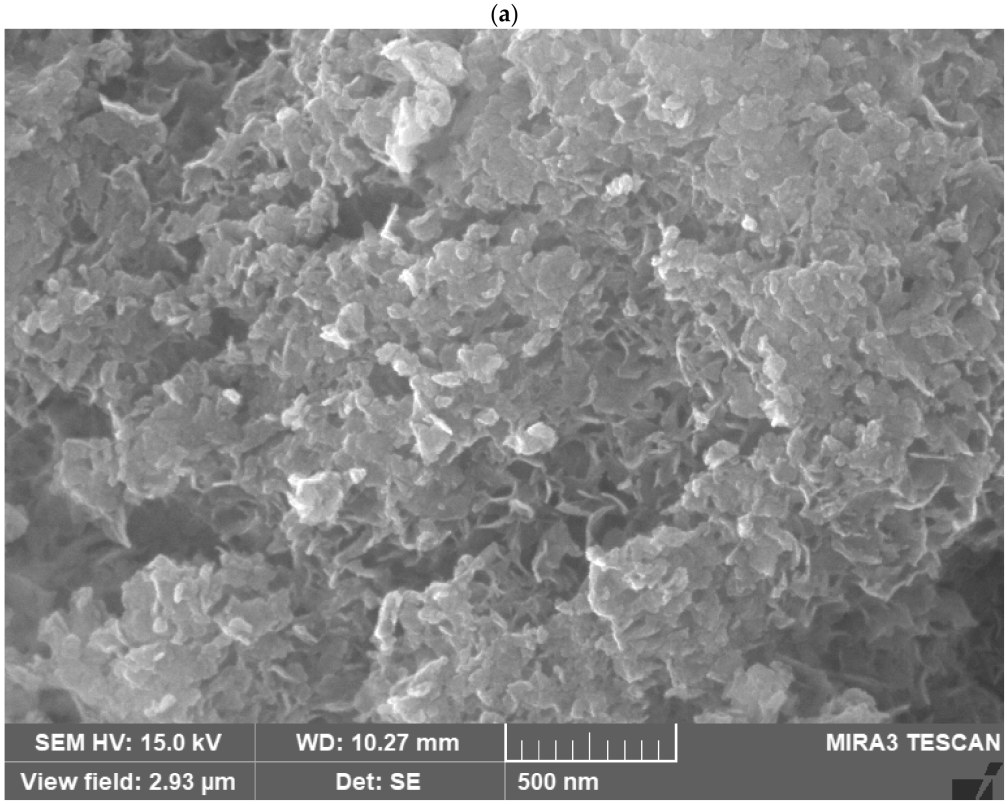
EDX Analysis

The EDX analysis of *C. roseus* flower-assisted MnO NPs confirmed the presence of manganese and oxygen as primary elements (Figure 6). The spectrum showed characteristic peaks for Mn at ~6.0 keV and O at ~0.5 keV, with quantitative elemental composition dominated by Mn (62.37%) and O (28.40%), along with minor contribution from C (9.23%) attributed to phytochemical capping agents using the flower extract. Majani et al. [43] exhibited via EDX mapping of *Saraca asoca* leaf extract-mediated MnO_2 NPs the atomic composition C (25%), O (47%), Mn (28%), with elevated oxygen linked to agglomerated

nanostructure development. *Musa paradisiaca* (Banana peel) mediated MnO NPs with 76 wt% Mn EDX along with K, Cl, Si, Ca, P and Zn impurities from the sample [44].



(**a**)



(**b**)

Figure 5. (**a**,**b**) FESEM of *C. roseus* flower-assisted MnO NPs.

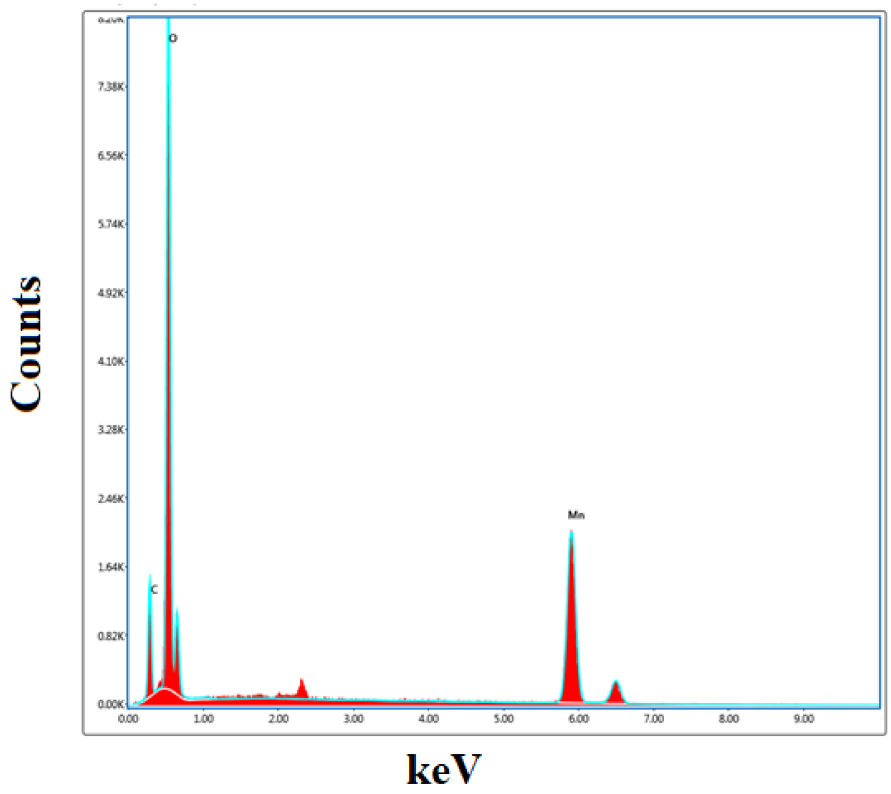


Figure 6. EDX analysis of *C. roseus* flower-assisted MnO NPs.

Zeta Potential Analysis

The zeta potential measurement of *C. roseus* flower-assisted MnO NPs revealed a value of −0.3 mV, indicating low electrostatic stabilization and low colloidal stability conferred by the negative surface charge from flower extract capping (Figure 7). Microfluidic tannic acid/PEG2000-reduced $KMnO_4$ yielded MnO_2 NPs with a zeta potential of -27.6 ± 0.4 mV, showing a strong colloidal stability with polyphenolic/PEG capping [45].

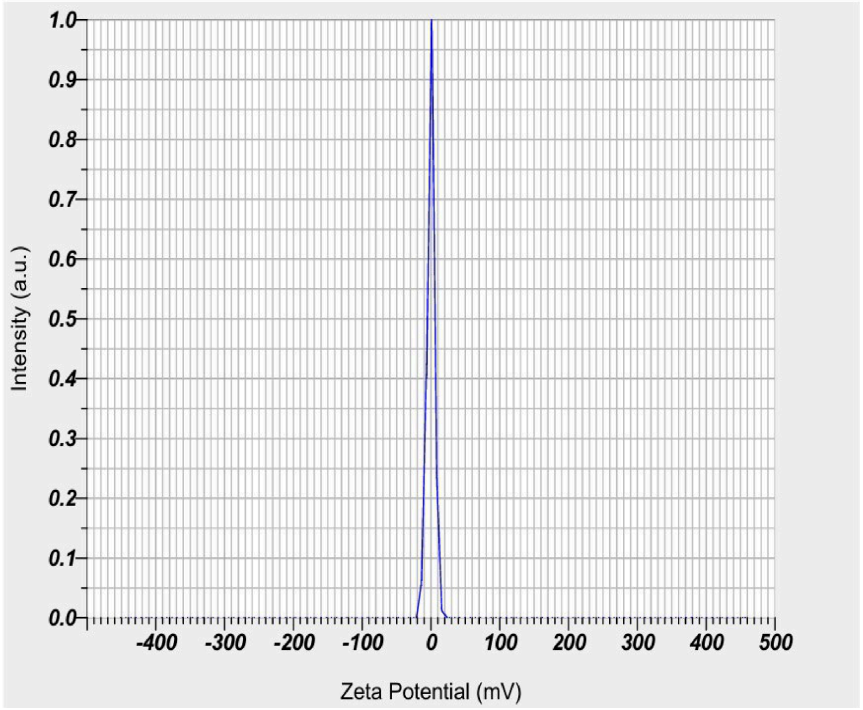


Figure 7. Zeta potential analysis of *C. roseus* flower-assisted MnO NPs.

TG Analysis

TG analysis of the *C. roseus* flower-assisted MnO NPs showed a total weight loss of 33.7% across three-stages: an initial 14.1% decrease between 30 and 250 °C due to removal of adsorbed moisture and volatile phytochemicals, a major 16.5% loss from 250 to 600 °C attributed to decomposition of more strongly bound organic constituents and conversion of residual manganese species, and a final 3.1% loss in the 600–985 °C range associated with burnout of persistent organic capping, indicating overall good thermal stability of the MnO core (Figure 8).

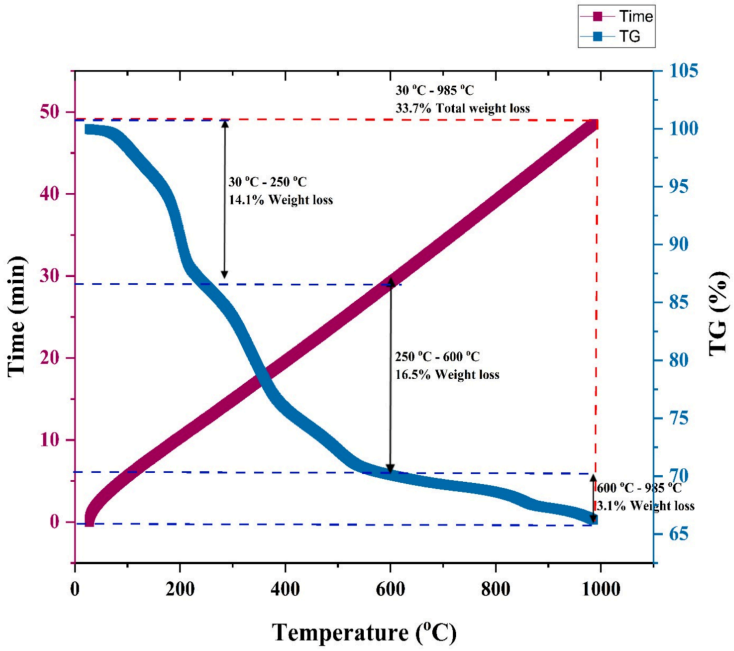


Figure 8. Thermogravimetric analysis of *C. roseus* flower-assisted MnO NPs.

Geetanjali et al. [46] documented steady TGA mass decline (30–600 °C) in *Sapindus mukorossi*-synthesized MnO_2 NPs attributed to water/organic decomposition, with DTA affirming thermal robustness via 72.16–100% mass retention. TGA curves of MnO nanorods synthesized using *Nelumbo nucifera* petal (NP) and *Rosa* petal (RP) extracts exhibited two-stage decomposition, with total weight losses of 31.4% (higher thermal stability) for NP and 50.8% (lower stability) for RP [47].

Antibacterial Activity

C. roseus flower-assisted MnO NPs displayed dose-dependent antibacterial efficacy, with inhibition zones of 10–15 mm against *K. pneumoniae*, 7–11 mm against *B. subtilis*, 10–13 mm against *E. coli* and 4–8 mm against *P. aeruginosa* at 40–100 µg/mL, surpassing ofloxacin 5 µg/disc controls. This activity stemmed from NP adhesion to bacterial surfaces, disrupting membranes and elevating ROS levels to impair cellular respiration and induce lysis (Figure 9). Karunakaran et al. [48] demonstrated that Mn_3O_4 NPs biosynthesized using *Chaenomeles* sp. flower extracts exhibited zones of inhibition of 16 ± 0.84 mm against *P. aeruginosa* (Gram-negative) and 15 ± 0.41 mm against *Streptococcus pyogenes* (Gram-positive) via Kirby–Bauer assay, surpassing streptomycin control and demonstrated higher efficacy against Gram-negatives due to thinner peptidoglycan layers. Kamran et al. [41] evidenced *Cinnamomum verum* bark extract-synthesized Mn NPs displayed concentration-dependent antimicrobial zones against *E. coli* (16 ± 0.5 to 22 ± 0.25 mm) > *S. aureus* (18 ± 0.7 to 4.5 ± 0.55 mm) at 0.4–1 mg/mL, nearing streptomycin (24 mm *S. aureus*, 27 mm *E. coli*) through Mn-thiol binding disrupting membrane permeability.

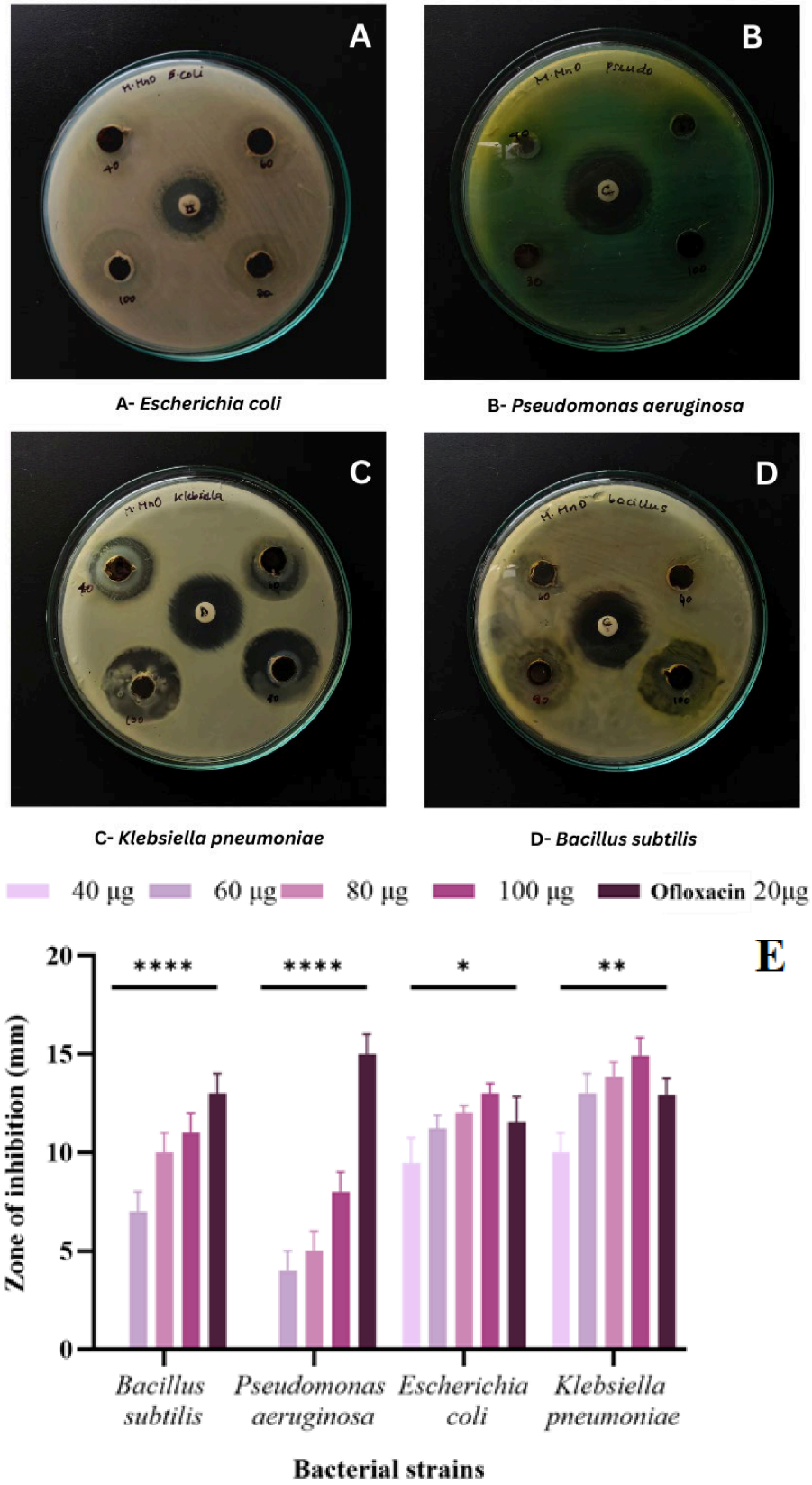


Figure 9. (**A**–**D**) Antibacterial activity of *C. roseus* flower-assisted MnO NPs. (**E**) Antibacterial activity of *C. roseus* flower-assisted MnO NPs. The antibacterial activity is assessed in triplicate ($n = 3$), and the zones of inhibition are measured in millimetres and reported as the mean ± standard deviation (SD). Statistical analysis is performed using a two-way ANOVA followed by a post hoc test, with statistical significance considered at **** $p < 0.0001$, ** $p < 0.01$, and * $p < 0.05$.

2.4.9. Cytotoxicity Assay

MTT assay on L929 fibroblast cells showed that *C. roseus*-assisted MnO NPs maintained 78.77% cell viability at 20 µg/mL, which decreased to 39.97% at 100 µg/mL. This effect arises from MnO NP-induced reactive oxygen species (ROS) generation, causing oxidative stress, mitochondrial dysfunction, and eventual apoptosis in fibroblasts. The triplicate measurements plotted in GraphPad Prism indicated a clear dose-dependent reduction in cell viability over the tested concentration range (Figure 10).

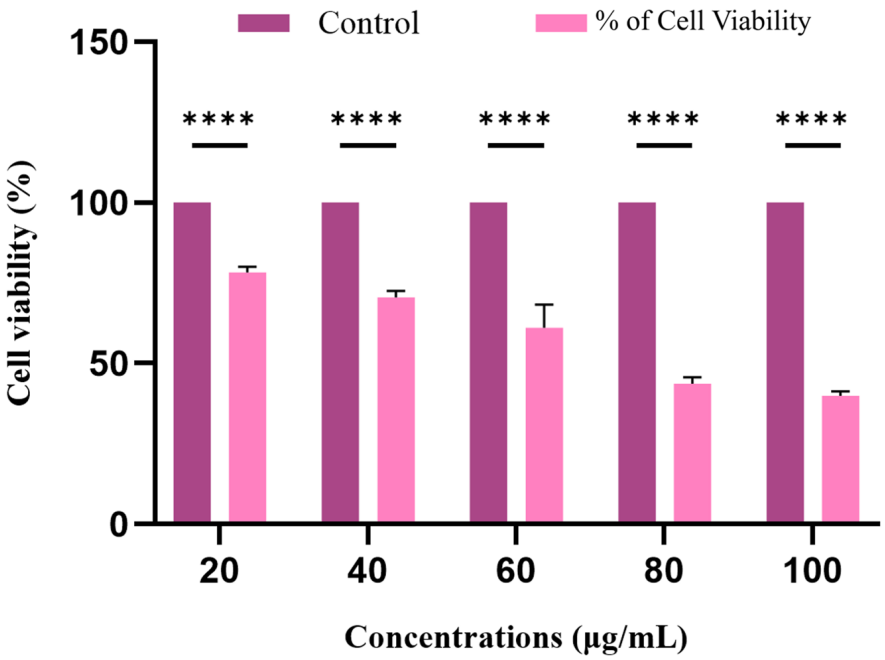


Figure 10. Cytotoxicity analysis of *C. roseus* flower-assisted MnO NPs. Statistical analysis was carried out using two-way ANOVA followed by a post hoc test, with statistical significance considered at **** $p < 0.0001$.

Z. clinopodioides mediated MnO NPs exhibited exceptional biocompatibility (>95% viability) against HUVEC cell line up to 1000 µg/mL after 48 h MTT assay, comparable to precursor $MnSO_4$ and extract controls [49]. Iacovita et al. [50] tested $MnFe_2O_4$ Polyol-Mediated NPs by four cell lines using MTT assay at concentrations of 0.05, 0.1, and 0.2 mg/mL for 24 h. No toxicity appeared at the lowest dose (0.05 mg/mL), viabilities dropped slightly to 98–91% at 0.1 mg/mL, and further to 80–95% at 0.2 mg/mL, with cancer cells showing greater sensitivity.

2.4.10. Scratch (Migration) Assay

Scratch assay on L929 fibroblasts revealed that *C. roseus*-assisted MnO NPs promoted cell migration (Figure 11), reducing the scratch area to −16.31% compared to −17.41% in untreated controls. At low concentrations, MnO NPs enhance fibroblast migration likely through mild ROS signalling that activates Matrix Metalloproteinases (MMPs) and growth factors, promoting wound healing without cytotoxicity.

Chitosan-Mn nanovesicles, synthesized via hydrothermal treatment, exhibited 57.84% wound closure in human dermal fibroblast (HDF) cell line at 16 µg/mL and (control: 49.30%) after 16 h in a cross-shaped scratch assay on confluent monolayers (1.3×10^5 cells/well) [51].

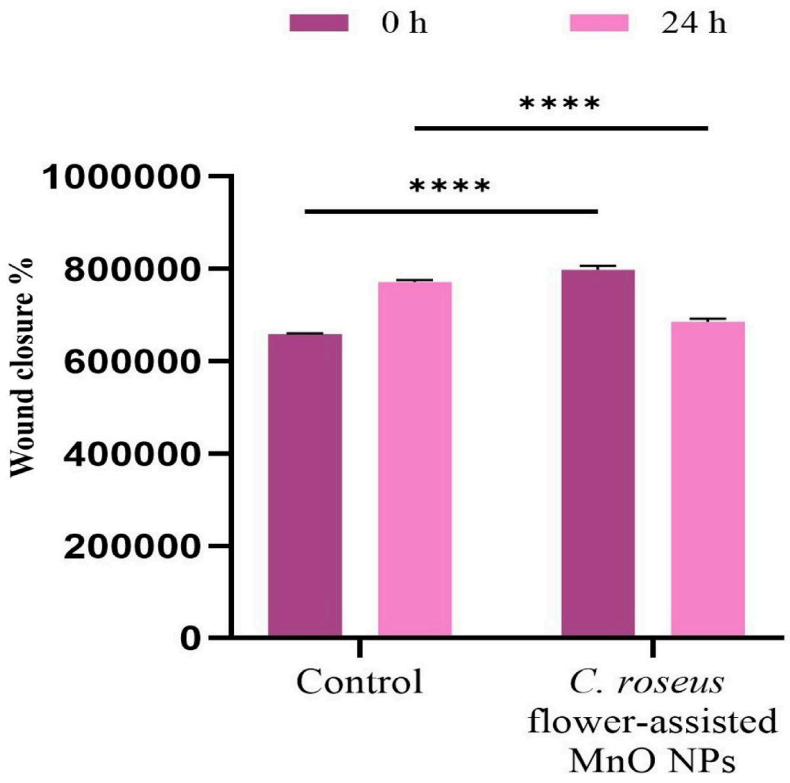


Figure 11. Wound healing-scratch assay of *C. roseus* flower-assisted MnO NPs. Statistical analysis is conducted using a two-way ANOVA followed by a post hoc test, with statistical significance considered at **** $p < 0.0001$.

3. Conclusions

The present work demonstrated that *C. roseus* flower extract was an effective biogenic platform for the synthesis of MnO NPs, yielding crystalline, thermally robust nanostructures with flaky, agglomerated morphology and moderate colloidal stability suitable for biological interfaces. Spectroscopic and microscopic analyses confirmed that phytochemical constituents participated in both the reduction of manganese precursors and coverage of the NPs surface, consistent with reports that plant-derived ligands can tune the physicochemical behaviour of green-synthesized metal and metal oxide nanomaterials for biomedical applications. In vitro evaluation on L929 fibroblasts showed that the *C. roseus*-mediated MnO NPs exerted a concentration-dependent reduction in cell viability, yet simultaneously promoted fibroblast migration in the scratch assay, a pattern consistent with the literature describing dose-window-dependent benefits of green-synthesized metal NPs in wound repair models. The *C. roseus*-mediated MnO NPs exhibited dose-dependent antibacterial efficacy, with the highest inhibition zones of 15 mm against *K. pneumoniae* and *E. coli*, and the lowest of 4 mm at 40–100 µg/mL. Collectively, these findings indicated that the biosynthesized MnO NPs possessed a promising balance between structural stability and bioactivity, supporting their further investigation as wound-healing adjuncts and broader regenerative or antimicrobial agents, with future work required to define optimal dosing, mechanisms of action, and in vivo therapeutic performance.

Author Contributions: R.P.: Conceptualization, supervision, funding acquisition and project administration; H.B.: investigation and writing—original draft preparation; V.P.: review and editing. J.A.M.: data curation; D.B.: data curation; N.A.-D.: data curation and software. All authors have read and agreed to the published version of the manuscript.

Funding: The authors have no relevant financial or non-financial interests to disclose.

Institutional Review Board Statement: Not applicable.

Informed Consent Statement: Not applicable.

Data Availability Statement: The original contributions presented in this study are included in the article. Further inquiries can be directed to the corresponding author.

Conflicts of Interest: The authors declare that they have no known competing financial interests or personal relationships that could have appeared to influence the work reported in this paper. The authors declare that they have no conflict of interest.

References

1. Omran, B.A. Fundamentals of Nanotechnology and Nanobiotechnology. In *Nanobiotechnology: A Multidisciplinary Field of Science*; Springer International Publishing: Cham, Switzerland, 2020; pp. 1–36. [CrossRef]
2. Chausali, N.; Saxena, J.; Prasad, R. Recent trends in nanotechnology applications of bio-based packaging. *J. Agric. Food Res.* **2022**, *7*, 100257. [CrossRef]
3. Taran, M.; Safaei, M.; Karimi, N.; Almasi, A. Benefits and application of nanotechnology in environmental science: An overview. *Biointerface Res. Appl. Chem.* **2021**, *11*, 7860–7870. [CrossRef]
4. Abobatta, W.F. Nanotechnology application in agriculture. *Acta Sci. Agric.* **2018**, *2*, 99–102.
5. Sindhwani, S.; Chan, W.C.W. Nanotechnology for modern medicine: Next step towards clinical translation. *J. Intern. Med.* **2021**, *290*, 486–498. [CrossRef]
6. Thiruvengadam, M.; Rajakumar, G.; Chung, I.-M. Nanotechnology: Current uses and future applications in the food industry. *3 Biotech.* **2018**, *8*, 74. [CrossRef]
7. Altammar, K.A. A review on nanoparticles: Characteristics, synthesis, applications, and challenges. *Front. Microbiol.* **2023**, *14*, 1155622. [CrossRef]
8. Sajid, M.; Płotka-Wasylka, J. Nanoparticles: Synthesis, characteristics, and applications in analytical and other sciences. *Microchem. J.* **2020**, *154*, 104623. [CrossRef]
9. Chavali, M.S.; Nikolova, M.P. Metal oxide nanoparticles and their applications in nanotechnology. *SN Appl. Sci.* **2019**, *1*, 607. [CrossRef]
10. Abid, N.; Khan, A.M.; Shujait, S.; Chaudhary, K.; Ikram, M.; Imran, M.; Haider, J.; Khan, M.; Khan, Q.; Maqbool, M. Synthesis of nanomaterials using various top-down and bottom-up approaches, influencing factors, advantages, and disadvantages: A review. *Adv. Colloid Interface Sci.* **2022**, *300*, 102597. [CrossRef]
11. Jiang, Z.; Li, L.; Huang, H.; He, W.; Ming, W. Progress in Laser Ablation and Biological Synthesis Processes: "Top-Down" and "Bottom-Up" Approaches for the Green Synthesis of Au/Ag Nanoparticles. *Int. J. Mol. Sci.* **2022**, *23*, 14658. [CrossRef]
12. Salem, S.S. A mini review on green nanotechnology and its development in biological effects. *Arch. Microbiol.* **2023**, *205*, 128. [CrossRef]
13. Nguyen, N.T.H.; Tran, G.T.; Nguyen, N.T.T.; Nguyen, T.T.T.; Nguyen, D.T.C.; Van Tran, T. A critical review on the biosynthesis, properties, applications and future outlook of green MnO_2 nanoparticles. *Environ. Res.* **2023**, *231*, 116262. [CrossRef]
14. Verma, A.; Gautam, S.P.; Bansal, K.K.; Prabhakar, N.; Rosenholm, J.M. Green Nanotechnology: Advancement in Phytoformulation Research. *Medicines* **2019**, *6*, 39. [CrossRef]
15. Hossain, A.; Manik, M.H.; Rakib, S.; Mahmud, N.; Khan, S.; Ahsan, Z.; Islam, M.S.; Hossain, N.; Akter, M.A. Green nanotechnology for implantable biosensors: Biocompatibility and functional integration in medical applications. *Biosens. Bioelectron. X* **2025**, *27*, 100678. [CrossRef]
16. Pandit, C.; Roy, A.; Ghotekar, S.; Khusro, A.; Islam, M.N.; Emran, T.B.; Lam, S.E.; Khandaker, M.U.; Bradley, D.A. Biological agents for synthesis of nanoparticles and their applications. *J. King Saud Univ. Sci.* **2022**, *34*, 101869. [CrossRef]
17. Schmidt, S.B.; Husted, S. The Biochemical Properties of Manganese in Plants. *Plants* **2019**, *8*, 381. [CrossRef]
18. Semenova, N.A.; Burmistrov, D.E.; Shumeyko, S.A.; Gudkov, S.V. Fertilizers based on nanoparticles as sources of macro-and microelements for plant crop growth: A review. *Agronomy* **2024**, *14*, 1646. [CrossRef]
19. Rastogi, A.; Zivcak, M.; Sytar, O.; Kalaji, H.M.; He, X.; Mbarki, S.; Brestic, M. Impact of metal and metal oxide nanoparticles on plant: A critical review. *Front. Chem.* **2017**, *5*, 78. [CrossRef]
20. Manavalan, R.K.; Enoch, K.; Volegov, A.S.; Angusamy, G.; Nallasivam, S. Review on Medical Applications of Manganese Oxide (Mn^{2+}, Mn^{3+}, and Mn^{4+}) Magnetic Nanoparticles. *J. Nanomater.* **2024**, *2024*, 1073915. [CrossRef]
21. Haleem, A.; Javaid, M.; Singh, R.P.; Rab, S.; Suman, R. Applications of nanotechnology in medical field: A brief review. *Glob. Health J.* **2023**, *7*, 70–77. [CrossRef]
22. Zhou, G.; Jin, X.; Chen, Z. Biosynthesis of manganese nanoparticles for efficient recovery of rare earth elements from mining wastewater. *J. Water Process Eng.* **2025**, *70*, 106987. [CrossRef]

23. Ogunyemi, S.O.; Zhang, F.; Abdallah, Y.; Zhang, M.; Wang, Y.; Sun, G.; Qiu, W.; Li, B. Biosynthesis and characterization of magnesium oxide and manganese dioxide nanoparticles using *Matricaria chamomilla* L. extract and its inhibitory effect on *Acidovorax oryzae* strain RS-2. *Artif. Cells Nanomed. Biotechnol.* **2019**, *47*, 2230–2239. [CrossRef]
24. Bhutekar, P.G.; Kshirsagar, A.K.; Bankar, S.S.; More, R.T. Green Synthesis of Manganese Dioxide and Copper Oxide Nanoparticles Using *Phaseolus lunatus* Flower Extract and Evaluation of Their Antimicrobial Activity. *Educ. Adm. Theory Pract.* **2024**, *30*, 3142–3148. [CrossRef]
25. Van Tran, T.; Nguyen, D.T.C.; Kumar, P.S.; Din, A.T.M.; Qazaq, A.S.; Vo, D.-V.N. Green synthesis of Mn_3O_4 nanoparticles using *Costus woodsonii* flowers extract for effective removal of malachite green dye. *Environ. Res.* **2022**, *214*, 113925. [CrossRef]
26. Gillani, S.S.; Khan, S.A.; Nazir, R.; Qurashi, A.W. Green Synthesis of Mixed Metal Oxide (MnO, CuO, ZnO) Nanoparticles (NPs) using Rose Petal Extract: An investigation of their Antimicrobial and Antifungal Activities. *Sci. Inq. Rev.* **2021**, *5*, 54–69. [CrossRef]
27. Sizov, L.R.; Serov, D.A.; Kozlov, V.A.; Karpov, V.A.; Yanbaev, F.M.; Gudkov, S.V. Review of Antimicrobial Properties of Carbon Nanomaterials. *Int. J. Mol. Sci.* **2026**, *27*, 4529. [CrossRef]
28. Negrescu, A.M.; Killian, M.S.; Raghu, S.N.V.; Schmuki, P.; Mazare, A.; Cimpean, A. Metal Oxide Nanoparticles: Review of Synthesis, Characterization and Biological Effects. *J. Funct. Biomater.* **2022**, *13*, 274. [CrossRef]
29. Pham, H.N.T.; Van Vuong, Q.; Bowyer, M.C.; Scarlett, C.J. Phytochemicals Derived from *Catharanthus roseus* and Their Health Benefits. *Technologies* **2020**, *8*, 80. [CrossRef]
30. Hira, F.A.; Islam, A.; Mitra, K.; Bithi, U.H.; Ahmed, K.S.; Islam, S.; Abdullah, S.M.; Uddin, M.N. Comparative Analysis of Phytochemicals and Antioxidant Characterization Among Different Parts of *Catharanthus roseus*: In Vitro and In Silico Investigation. *Biochem. Res. Int.* **2024**, *2024*, 1904029. [CrossRef]
31. Pandey, S.N.; Pratap, V.; Pratap, S.; Kumar, N. Phytochemicals And Pharmacological Studies Of *Catharanthus roseus* Linn-A Comprehensive Review. *World J. Pharm. Res.* **2020**, *9*, 1407–1415.
32. Don, L.G.; Sharma, P.; Singla, N.; Kaur, R.; Bhardwaj, U. A review on phytochemical constituents and pharmacological properties of *Catharanthus roseus* (L.) G. Don. *J. Med. Plants Stud.* **2024**, *12*, 131–156. [CrossRef]
33. Kandiah, M.; Chandrasekaran, K.N. Green Synthesis of Silver Nanoparticles Using *Catharanthus roseus* Flower Extracts and the Determination of Their Antioxidant, Antimicrobial, and Photocatalytic Activity. *J. Nanotechnol.* **2021**, *2021*, 5512786. [CrossRef]
34. Akpeji, B.H.; Lari, B.; Igbuku, U.A.; Tesi, G.O.; Elemike, E.E.; Akusu, P.O. Synthesis and characterization of MnO_2 nanoparticles mediated by *Raphia hookeri* seed. *J. Niger. Soc. Phys. Sci.* **2024**, *6*, 2203. [CrossRef]
35. Thangapushbam, V.; Rama, P.; Sivakami, S.; Jothika, M.; Muthu, K.; Almansour, A.I.; Arumugam, N.; Perumal, K. Potential in-vitro antioxidant and anti-inflammatory activity of *Martynia annua* extract mediated Phytosynthesis of MnO_2 nanoparticles. *Heliyon* **2024**, *10*, e29457. [CrossRef]
36. Alshahrani, D.O.; Khan, H.; Saad, M. Boosting energy storage performance of green-synthesized MnV_2O_5 via jasmine flower extract as natural and stabilizing agent. *Results Phys.* **2025**, *76*, 108389. [CrossRef]
37. Vanitha, A.; Kalimuthu, K.; Chinnadurai, V.; Nisha, K.M.J. Phytochemical screening, FTIR and GCMS analysis of aqueous extract of *Caralluma bicolor*–An endangered plant. *Asian J. Pharm. Pharmacol.* **2019**, *5*, 1122–1130. [CrossRef]
38. Valle-Rivera, E.; Jáuregui-Rosas, S.R.; Avila-Concepción, S.P.R.; Samanamud-Moreno, F.V.; Zavaleta-Espejo, G.G.; Huaman-Quispe, J.; Gavidia-Sare, S.; Saldaña-Jiménez, J.A.; Valle-Rivera, E.; Jáuregui-Rosas, S.R.; et al. Biosynthesis and Characterization of Mn_3O_4 Nanoparticles Using *Bixa orellana* and *Nerium oleander* Leaf Extracts at Low Temperature and Neutral pH. *Crystals* **2025**, *15*, 226. [CrossRef]
39. Dixit, A.; Bala, R.; Pareek, B.; Chaudhary, A.; Jaswal, V.S. An analysis of green synthesis of manganese oxide nanoparticles including applications and prospects as anticancer activity (MTT, ROS & MMP). *Int. J. Bot. Stud.* **2021**, *6*, 1452–1456.
40. Mahlangeni, N.T.; Moodley, R. Biosynthesis of manganese oxide nanoparticles using *Urginea sanguinea* and their effects on cytotoxicity and antioxidant activity. *Adv. Nat. Sci. Nanosci. Nanotechnol.* **2021**, *12*, 15015. [CrossRef]
41. Kamran, U.; Bhatti, H.N.; Iqbal, M.; Jamil, S.; Zahid, M. Biogenic synthesis, characterization and investigation of photocatalytic and antimicrobial activity of manganese nanoparticles synthesized from *Cinnamomum verum* bark extract. *J. Mol. Struct.* **2019**, *1179*, 532–539. [CrossRef]
42. Hussain, S.; Aslam, A.; Tajammal, A.; Othman, F.; Mustafa, Z.; Alsuhaibani, A.M.; Refat, M.S.; Shahid, M.; Sagir, M.; Zakaria, Z.A. *Tagetes erecta*-Mediated Biosynthesis of Mn_3O_4 Nanoparticles: Structural, Electrochemical, and Biological Investigations. *ACS Omega* **2024**, *9*, 35408–35419. [CrossRef]
43. Majani, S.S.; Sathyan, S.; Manoj, M.V.; Vinod, N.; Pradeep, S.; Shivamallu, C.; Venkatachalaiah, K.N.; Kollur, S.P. Eco-friendly synthesis of MnO_2 nanoparticles using *Saraca asoca* leaf extract and evaluation of in vitro anticancer activity. *Curr. Res. Green Sustain. Chem.* **2023**, *6*, 100367. [CrossRef]
44. Amatya, S.P.; Shrestha, S.; Aryal, Y. Green Approach for Synthesis of Manganese Nanoparticle using Banana Peel (*Musa paradiasca*) and its Characterization. *Amrit Res. J.* **2021**, *2*, 75–82. [CrossRef]
45. Wang, X.; Yang, X.; Yi, X.; Min, X.; Jia, Y. Rapid synthesis of manganese dioxide nanoparticles for enhanced biocompatibility and theranostic applications. *RSC Adv.* **2025**, *15*, 3060–3065. [CrossRef]

46. Lohiya, G.; Tamta, A.; Chandra, B.; Kandpal, N.D.; Joshi, R. Green route synthesis of manganese oxide nanoparticles by using methanolic extract of *Sapindus mukorossi* (reetha). *J. Water Environ. Nanotechnol.* **2024**, *9*, 211–222. [CrossRef]
47. Syed Khadar, Y.A.; Surendhiran, S.; Gowthambabu, V.; Halimabi Alias Shakila Banu, S.; Devabharathi, V.; Balamurugan, A. Enhancement of corrosion inhibition of mild steel in acidic media by green-synthesized nano-manganese oxide. *Mater. Today Proc.* **2021**, *47*, 889–893. [CrossRef]
48. Karunakaran, G.; Jagathambal, M.; Kolesnikov, E.; Dmitry, A.; Ishteev, A.; Gusev, A.; Kuznetsov, D. Floral Biosynthesis of Mn_3O_4 and Fe_2O_3 Nanoparticles Using *Chaenomeles* sp. Flower Extracts for Efficient Medicinal Applications. *JOM* **2017**, *69*, 1325–1333. [CrossRef]
49. Mahdavi, B.; Paydarfard, S.; Zangeneh, M.M.; Goorani, S.; Seydi, N.; Zangeneh, A. Assessment of antioxidant, cytotoxicity, antibacterial, antifungal, and cutaneous wound healing activities of green synthesized manganese nanoparticles using *Ziziphora clinopodioides* Lam leaves under in vitro and in vivo condition. *Appl. Organomet. Chem.* **2020**, *34*, e5248. [CrossRef]
50. Iacovita, C.; Florea, A.; Scorus, L.; Pall, E.; Dudric, R.; Moldovan, A.I.; Stiufiuc, R.; Tetean, R.; Lucaciu, C.M. Hyperthermia, Cytotoxicity, and Cellular Uptake Properties of Manganese and Zinc Ferrite Magnetic Nanoparticles Synthesized by a Polyol-Mediated Process. *Nanomaterials* **2019**, *9*, 1489. [CrossRef]
51. Davidson, E.; Pereira, J.; Gan Giannelli, G.; Murphy, Z.; Anagnostopoulos, V.; Santra, S. Multi-Functional Chitosan Nanovesicles Loaded with Bioactive Manganese for Potential Wound Healing Applications. *Molecules* **2023**, *28*, 6098. [CrossRef]

Disclaimer/Publisher's Note: The statements, opinions and data contained in all publications are solely those of the individual author(s) and contributor(s) and not of MDPI and/or the editor(s). MDPI and/or the editor(s) disclaim responsibility for any injury to people or property resulting from any ideas, methods, instructions or products referred to in the content.